A Platform for All-Optical Thomson/Compton Scattering with Versatile Parameters

Siyu Chen[1], Wenchao Yan[1,3], Mingyang Zhu[1], Yaojun Li[1], Xichen Hu[1], Hao Xu[1], Weijun Zhou[1], Guangwei Lu[1], Mingxuan Wei[1], Lin Lu[1,3], Xulei Ge[1,2,3], Boyuan Li[1,3], Xiaohui Yuan[1,3], Feng Liu[1,3], Min Chen[1,3], Liming Chen[1,3], and Jie Zhang[1,2,3]

[1]*State Key Laboratory of Dark Matter Physics, Key Laboratory for Laser Plasmas (MoE), School of Physics and Astronomy, Shanghai Jiao Tong University, Shanghai 200240, China.*
[2]*Tsung-Dao Lee Institute, Shanghai Jiao Tong University, Shanghai 201210, China.*
[3]*Collaborative Innovation Center of IFSA, Shanghai Jiao Tong University, Shanghai 200240, China.*

Abstract
A dual-beam platform is developed for all-optical Thomson/Compton scattering, with versatile parameter tuning capabilities including electron energy, radiation energy, radiation polarization, etc. By integrating this platform with a 200 TW Ti: Sapphire laser system, we demonstrate the generation of inverse Compton scattering X/gamma-rays with tunable energies ranging from tens of keV to MeV. The polarization of X/gamma-rays is manipulated by adjusting the polarization of the scattering laser. In the near future, by combining this platform with multi-PW laser facilities, our goal is to explore the transition from nonlinear Thomson scattering to nonlinear Compton scattering, ultimately verifying theories related to strong-field quantum electrodynamics effects induced by extreme scattering.

Keywords: inverse Compton scattering, strong-field QED, platform, X/gamma-ray

1. Introduction

The investigation of strong-field quantum electrodynamics (SF-QED) processes requires extreme field intensities approaching the Schwinger limit[1], which cannot be reached by state-of-the-art laser facilities. However, when a relativistic electron travels through an existing intense laser field, the field experienced by the electron in its rest frame is Lorentz transformed to a level where SF-QED effects matter. Therefore, relativistic electrons can act as probes to test these effects. This interaction is known as Thomson or Compton scattering, depending on whether the process is elastic or inelastic scattering. During the scattering, collimated X/gamma-rays are generated and can be used as radiation sources, commonly known as the inverse Compton scattering (ICS) source. Previously, scattering experiments were conducted in the laboratories of particle accelerators, but the remarkable advances in laser wakefield acceleration (LWFA)[2] have now enabled the study of these experiments under the all-optical setup within high-intensity laser laboratories. The principle of the scattering process is shown in Figure 1.

Correspondence to: Wenchao Yan, State Key Laboratory of Dark Matter Physics, Key Laboratory for Laser Plasmas (MoE), School of Physics and Astronomy, Shanghai Jiao Tong University, Shanghai 200240, China. Email: wenchaoyan@sjtu.edu.cn

There are two possible configurations for all-optical scattering experiments. One is a simplified version that involves only one laser beam. This laser beam first drives a wakefield accelerator, and then the leftover energy of it is reflected by a plasma mirror[3–10] onto electrons, causing head-on scattering. The other scheme features a layout with two independently tunable laser pulses[5,11–18]. Although precise temporal and spatial synchronization between the two beamlines is technically difficult, the dual-beam scheme offers the distinct advantage of independently controlling the properties of the scattering process. Each of the two lasers can be individually tuned to optimal conditions, enabling the generation of high-energy electrons and the scattering laser that meets specific requirements, respectively. Specifically, by maintaining the parameters of the LWFA constant, one can exclusively manipulate the colliding pulse, enabling a single-variable investigation into the scattering process.

To investigate these scattering processes, we established an experimental platform for dual-beam all-optical Thomson/Compton scattering (EPATCS) with versatile parameter tuning capabilities. The EPATCS is a tabletop electron-photon interaction setup, where high-energy electrons are accelerated by one laser beam and then collide with the

10.1017/hpl.2025.36

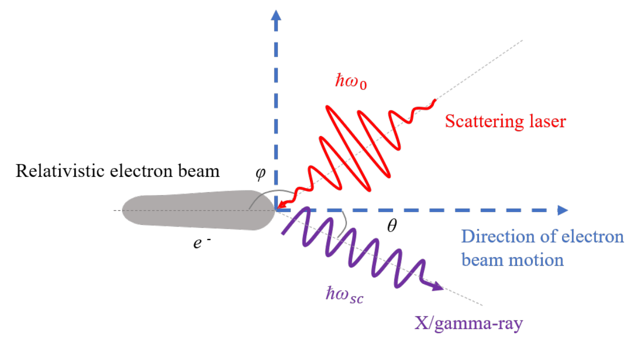

Figure 1. Schematic diagram of Thomson/Compton scattering process. A relativistic electron beam collides with a scattering laser. The electrons oscillate and emit X/gamma-rays. φ denotes the collision angle between the laser and the electron beam, while θ represents the radiation observation angle. γ_e refers to the Lorentz factor of electron, ω_0 signifies the central frequency of the scattering laser photon, and ω_{sc} corresponds to the frequency of the emitted photon.

second laser beam. The flexibility in parameter tuning not only enhances control over experimental conditions, but also opens up new prospects for investigating high-field scattering processes. By precisely controlling the intensity, polarization state, and field mode of the colliding laser beam, we can generate X/gamma-rays with varying characteristics, which can serve as light sources for applications such as high-density dynamic imaging[19–26] and vortex photons for photonuclear physics[27,28]. The EPATCS can also be built on the PW laser facilities and provides the possibility of the interaction between multi-GeV electrons and high laser intensity under extreme conditions[18] to study SF-QED effects, including radiation reaction[11,12], pair production[10,29–31], and conversion of angular momentum transfer in the collision process[32–34], etc.

This paper is organized as follows. In Section 2, we discuss the versatile tuning of ICS X/gamma-ray source parameters and their impact on enhancing control over high-field processes and tunable radiation spectra. Section 3 presents the experimental results based on the EPATCS at the 200-TW laser in Shanghai Jiao Tong University. In Section 4, we elucidate the prospective SF-QED research of EPATCS.

2. Versatile tuning parameters of EPATCS

EPATCS offers the potential for multi-parameter adjustments, including tuning the electron beam energy, altering the collision angle between electrons and photons, and adjusting the parameters of the colliding laser (such as laser intensity, wavelength, polarization, orbital angular momentum, etc.). In this section, we introduce the experimental designs and explorations to investigate the adjustable parameters and their effects on radiation.

A schematic diagram of a dual-beam collision layout was designed, as shown in Figure 2 (a), to investigate the influence of multiple parameters on the photon energy of radiation in the ICS process. The combination of the optical system and guide rail enables precise adjustments to the electron-laser collision angle. Adjustments in the collision angle φ, the focusing intensity a_0, the wavelength λ, the polarization state P and the orbital angular momentum $\vec{L}$ of the colliding beam will significantly alter the characteristics of the radiation emitted. Adjusting the collision angle φ results in a significant variation in the energy spectrum of the X/gamma-ray covers tens of keV to MeV[35]. When the normalized vector potential of the colliding laser, a_0, varies from less than 1 to greater than 1, the electron-photon interaction shifts from linear to nonlinear process[13,16,17]. Modifying the wavelength λ alters the colliding laser photon energy $E_0 = \hbar c/\lambda$, which in turn modifies the energy of the scattered photons, that is, the radiation energy[15]. Since this is a fundamental model of a scattering process, the polarization state of the colliding laser directly influences the polarization of the emitted radiation[9]. When the colliding laser is transformed from a Gaussian laser to a Laguerre-Gaussian laser, adjustments in the orbital angular momentum directly affect the orbital angular momentum of the X/gamma radiation[32,36].

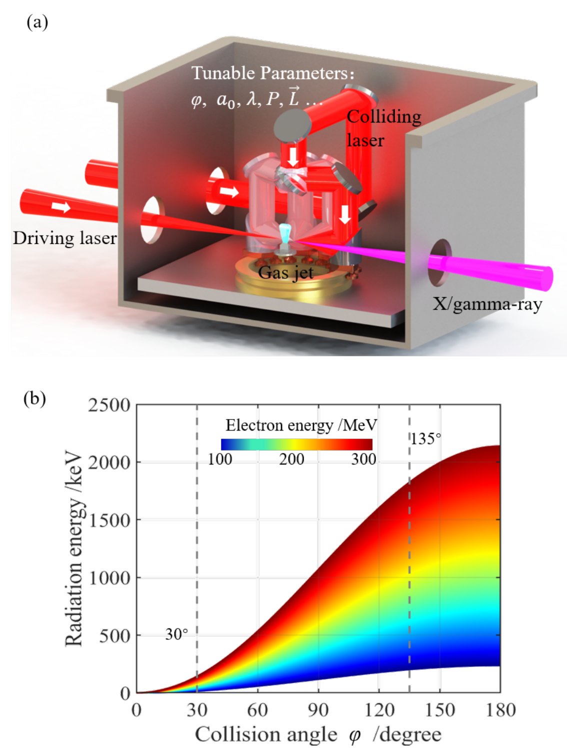

Figure 2. (a) The schematic diagram of the experimental layout with multiple collision angles. (b) represents the radiation energy under different collision angles φ with electron energy from 100 MeV (blue) to 300 MeV (red) when the observed angle $\theta = 0$. The cases of 30° and 135° are specifically marked to correspond with the experimental results discussed later in Section 3.2.

To illustrate this principle with a specific example, ad-

https://doi.org/10.1017/hpl.2025.36 Published online by Cambridge University Press

justing the collision angle demonstrates how changes in laser parameters can regulate radiation. In the ICS process, altering the collision angle between electrons and photons can significantly modify the energy spectrum of the emitted radiation. The energy of the emitted photon E_{sc} can be expressed by[37]:

$$E_{sc} = E_0 \frac{2n\gamma_e^2(1-\cos\varphi)}{1+a_0^2/2+\gamma_e^2\theta^2} \qquad (1)$$

where n represents the nonlinear order, E_0 represents the incident photon energy. γ_e denotes the Lorentz factor of electron, $a_0 = eA_0/m_e c$ is the normalized amplitude of the vector potential, e and m_e are the elementary charge and the rest mass of the electron. According to Equation (1), the energy of the scattered photons is correlated with that of the incident photons in the following manner, $E_{sc} \sim E_0\gamma_e^2\eta$, where $\eta = 1-\cos\varphi$ is a parameter related to the collision angle, exhibiting a clear range from 0 to 1. Therefore, altering the collision angle acts as an effective approach to enable the continuous adjustability of the ICS radiation energy range. Figure 2 (b) illustrates the radiation energy at the observation angle of $\theta = 0$ generated by linear ICS at various collision angles for electron energies ranging from 100 to 300 MeV.

In Section 3, the collision angle φ and the polarization state of the colliding laser are altered to validate the feasibility of this platform. In Section 3.2, the ICS processes are experimentally validated at collision angles of 30° and 135°, corresponding to the theoretical values calculated in Figure 2 (b), and the corresponding radiation energy spectra are diagnosed and analyzed.

3. X/gamma-ray manipulation by EPATCS on a 200TW laser

To validate the applicability of the EPATCS, it was initially integrated into the 200 TW Ti: sapphire laser facility at the Laboratory for Laser Plasma in Shanghai Jiao Tong University. A total of 5 J p-polarized laser pulse with a duration of $\tau = 25$ fs (full width at half maximum, FWHM) can be delivered to the target. The schematic diagram of the experimental setup and its primary components are referenced in Appendix B.

3.1. *Energy tunability of X/gamma-ray via LWFA electron*

The laser pulse for LWFA is focused by an off-axis parabolic mirror of F#20 to a Gaussian-like spot size, containing 30% energy with a FWHM diameter of 26 μm, and the focused laser intensity can reach up to 5×10^{18} W · cm^{-2}, corresponding to a normalized vector potential of $a_0 = 2$. The laser was focused above a supersonic gas jet of nitrogen. The electron energy can be effectively adjusted by modifying the relative position of the nozzle and the laser focus and adjusting the plasma density.

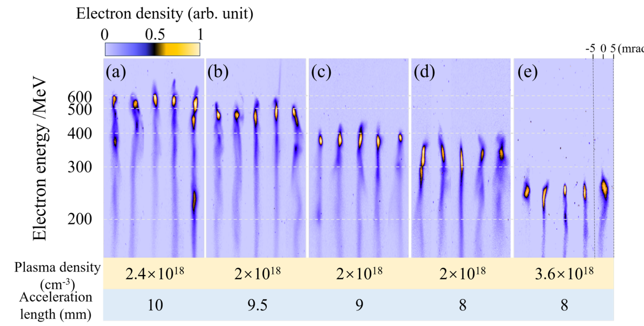

Figure 3. The diagnosis results of the electron beam with different acceleration lengths or plasma densities. From (a) to (e), the corresponding plasma densities are 2.4×10^{18}cm^{-3}, 2×10^{18}cm^{-3}, 2×10^{18}cm^{-3}, 2×10^{18}cm^{-3}, and 3.6×10^{18}cm^{-3} respectively, with acceleration lengths of 10 mm, 9.5 mm, 9 mm, 8 mm, and 8 mm.

As shown in Figure 3, consistent energy electron beams, tunable within the range of 200 to 600 MeV, can be achieved under stable conditions. For each scenario, the plasma density and acceleration length are indicated, resulting in relatively stable electron energy spectra. Under appropriate plasma density, decreasing the acceleration length within a certain range can effectively enhance the energy of relativistic electrons. The corresponding electron spectrum is shown in Figure 3 (a), (b), (c) and (d). However, as shown in Figure 3 (d) and (e), when the plasma density is significantly increased, the phase velocity of the wakefield decreases, causing the electrons to dephase earlier, leading to a reduction in their energy. Based on the scale shown in Figure 3 and the actual distance of the image plate from the target, which is 1.6 meters, the transverse divergence angle of the electron bunch is approximately 3 mrad (FWHM).

The tuning energy of the electron enables the radiation energy spectrum to span a wide range. As indicated in Equation (1), when $a_0 \ll 1$ (linear scattering regime), the energy of the emitted photon E_{sc} is directly proportional to the square of the electron Lorentz factor γ_e, a relationship that has been verified in several laboratories[13,16,38]. Figure 2 (b) demonstrates that under a fixed collision angle, the radiation energy spectrum varies accordingly with changes in electron energy.

3.2. *Energy control of X/gamma-ray by interaction angle*

In the scattering experiments, the relativistic electrons generated by LWFA have a cut-off energy of approximately 300 MeV, approaching a continuous spectrum. Two experimental configurations with collision angle of $\varphi = 30^\circ$ and $\varphi = 135^\circ$ are set, as shown in Figure 4 (a) and (b). The colliding beam is derived from the main laser pulse using a small pick-up mirror and is focused to a spot with an 8 μm full width at half maximum. With a pulse energy of 200 mJ and a pulse duration of 25 fs, the on-target peak

https://doi.org/10.1017/hpl.2025.36 Published online by Cambridge University Press

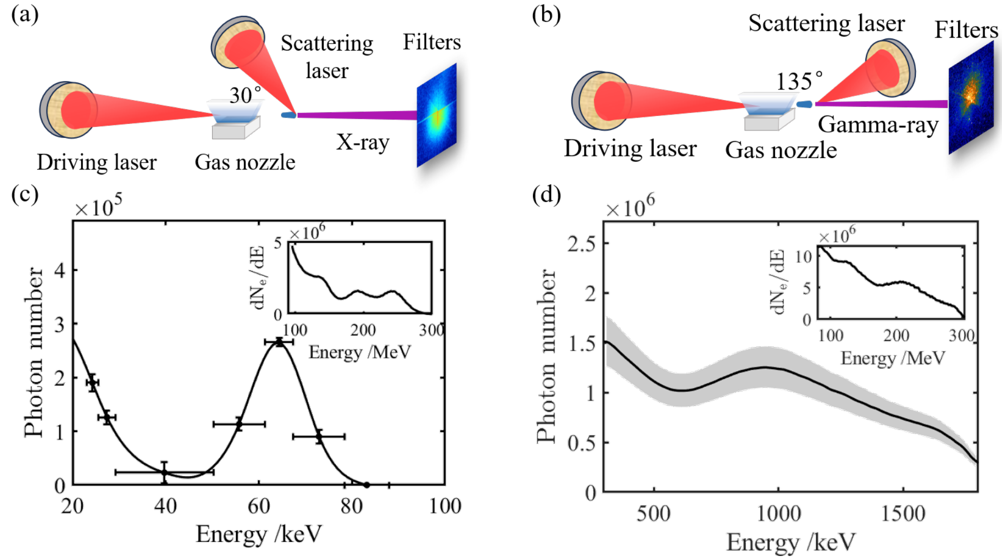

Figure 4. (a) and (b) are the experimental layout diagrams of AOICS under two conditions of 30° and 135° collision angles. (c) and (d) represent the radiation spectra with errorbars for collision angles of 30° and 135°, respectively. The corresponding electron energy spectra for each instance are displayed in the upper right corner of the graphs.

intensity is approximately $4.8 \times 10^{18}\ \mathrm{W \cdot cm^{-2}}$. The range of the radiation spectrum can be determined by altering the collision angle using Eq. (1). Metal filter sheets of various materials and thicknesses are designed for radiation diagnosis.

In the experimental setup with a collision angle of 30°, Ross-Filter pairs were selected on the basis of the K-absorption edges of metal filters with varying materials and thicknesses. The signal on the image plate behind the filters was obtained from a single shot. Using the least-squares method, we obtained convergence results and derived the energy spectrum. As shown in Figure 4 (c), the quasi-monoenergetic peak of the X-ray spectrum at around 65 keV might come from the ICS involving only a subset of electrons. When the electron beam interacts with the laser beam at a small angle, their velocities become comparable, causing the laser pulse to continuously interact with the same portion of the electrons within the Rayleigh length. Consequently, it results in the production of quasimonochromatic X-rays.

In the case of a collision angle 135°, the radiation energy spectrum extends beyond 1 MeV. The intensity distribution of the high-resolution CsI fluorescence from a single shot, located behind the filters, was captured by a 16-bit Andor Electron-Multiplying Charge-Coupled Device. The iterative least squares method is adopted for the numerical analysis of the transmission coefficient [39] to calculate the final energy spectrum of the X-rays, as illustrated in Figure 4 (d). Variations in the collision angle impact the radiation energy spectrum, which is directly influenced by the electron energy spectrum. The basic principles of spectrum diagnostics can be referred to in Appendix A.

3.3. *Polarization control of X/gamma-ray*

Polarized X-rays can be used to probe the characteristics of magnetic structures in structural magnetism and distinguish between chiral and helical magnetic structures [40–44]. Based on EPATCS, we generate polarized X-rays via the collision of a polarized laser beam and the electrons. As shown in Figure 5 (a), a half-wave plate or a quarter-wave plate is incorporated into the scattering laser path to change the polarization state of the scattering laser, which in turn modifies the polarization state of the generated radiation. An off-axis parabolic mirror of F#5 is used to focus the colliding laser. Under linear polarization conditions, the focal spot diameter and laser intensity are the same as those presented in Section 3.2, whereas under circular polarization, the laser intensity is approximately $2.4 \times 10^{18}\ \mathrm{W \cdot cm^{-2}}$. The collision angle is 135° and the experimental layout is illustrated in Figure 5 (a).

As shown in Figure 5 (a), a cylindrical polyethylene converter with a diameter of 2 cm and a length of 15 cm is placed 1.9 m from the impact point, and four image plates are placed around the converter. The secondary photon signal radiated on the scatterer is diagnosed in the vertical direction of X-ray propagation based on the Compton scattering. When the scattering angle is close to 90°, the azimuth distribution of scattered photons is highly dependent on X-ray polarization, making Compton scattering effective for the diagnosis of polarization [45]. The expressions of the scattering cross section of Compton scattering in the vertical direction of propagation for linear polarization [see Equation (2)] and circular polarization [see Equation (3)] are

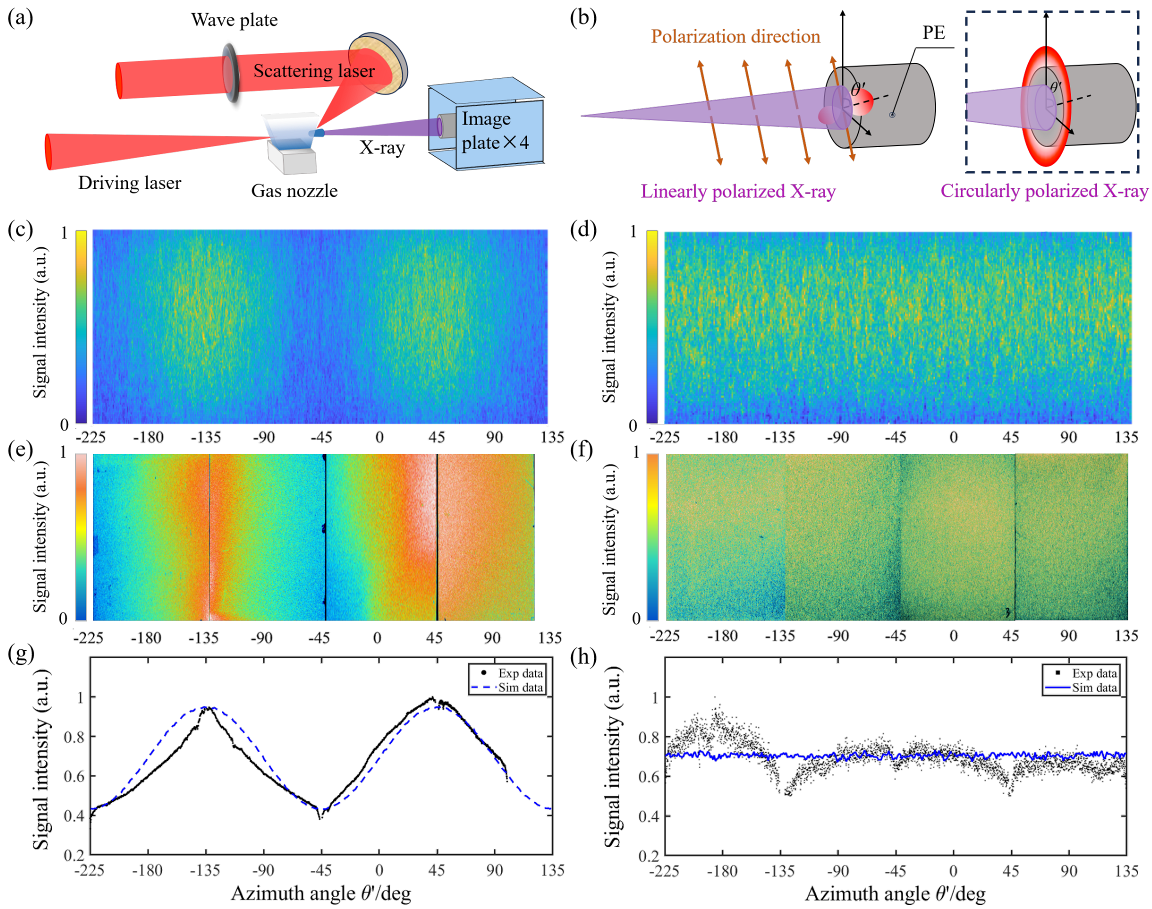

Figure 5. (a) Experimental layout. The polarization state of the X-ray was obtained by placing the polyethylene forward in the X-ray and placing four image plates around it to diagnose the signal scattered by the scattering in different polarization states. (b) Schematic representation of Compton scattering of linearly/circularly polarized X-rays with polyethylene (PE) scatterers. The red portions indicate the distribution direction of the scattered electrons. (c) and (d) show the simulation results by FLUKA, corresponding to the respective Compton scattering signals of linearly polarized and circularly polarized X-rays with polyethylene. (e) and (f) are the experimental diagnostic results of linearly polarized and circularly polarized X-rays, respectively. In (g) and (h), the signal image formed by black dots is the one-dimensional integral result of the experimental results, and the dashed blue line represents the simulation results.

as follows[46]:

$$\frac{\mathrm{d}\sigma_{\mathrm{lin}\perp}}{\mathrm{d}\Omega} = \frac{1}{4} r_{\mathrm{e}}^2 \left(\frac{\varepsilon}{\varepsilon_0}\right)^2 \left[\frac{\varepsilon}{\varepsilon_0} + \frac{\varepsilon_0}{\varepsilon} - 2\cos^2\theta'\right] \tag{2}$$

$$\frac{\mathrm{d}\sigma_{\mathrm{cir}\perp}}{\mathrm{d}\Omega} = \frac{1}{4} r_{\mathrm{e}}^2 \left(\frac{\varepsilon}{\varepsilon_0}\right)^2 \left[\frac{\varepsilon}{\varepsilon_0} + \frac{\varepsilon_0}{\varepsilon}\right] \tag{3}$$

where r_e represents the classical radius of the electron, where ε_0 is the energy of the incident photon, ε the energy of the scattered photon, and θ' denotes the scattering azimuth angle. According to Equation (2), Compton scattering of linearly polarized X-rays through the scatterer in the vertical direction is a function of the azimuth angle θ'. When the incident X-ray is circularly polarized, Equation (3) reveals that the vertical Compton scattering is independent of the azimuth angle θ'. In the experiment, the optical axis of the half-wave plate is adjusted to an angle of 22.5° from the original horizontal polarization direction, thus producing a linear polarization angle of 45° from the horizontal direction, as shown in Figure 5 (b). The reason behind this choice of angle is to facilitate differentiation of the background signal. Due to the wide spectral width of the laser and the bandwidth limitations of the quarter-wave plate, the conversion efficiency of linearly polarized light to circularly polarized light is approximately 80%.

We conducted simulations using FLUKA to simulate the process, and the results are shown in Figure 5 (c) and (d) and the experimental results are shown in Figure 5 (e) and (f). Each result accumulated 100 shots, which facilitated the diagnosis of the polarization characteristics of the radiation through the scattered electron distribution. The four image plates are arranged to correspond to azimuth angles ranging from -225° to 135°, with the portion corresponding to 100°-135° being absent, due to constraints on the size of the image plate. Figure 5 (g) and (h) include both theoretical simulation results and experimental data,

https://doi.org/10.1017/hpl.2025.36 Published online by Cambridge University Press

with normalized intensity signals. The linear polarization diagnostics show a periodic intensity distribution across the four image plates, indicative of a Compton scattering signal corresponding to the scatters of linearly polarized X-rays. The generated linearly polarized radiation spectrum is illustrated in Figure 4(b). The degree of polarization $(I_{\max} - I_{\min})/(I_{\max} + I_{\min})$ according to the experimental results is about 0.42, and the background greatly influenced this result. Moreover, the diagnostic results of circularly polarized X-rays exhibit uniformly distributed intensity signals overall, although a weak periodic intensity distribution signal is still observed near -180°. This suggests that the degree of polarization of circularly polarized X-rays generated by the ICS is not 100%, but rather an elliptical polarization state along the transverse axis. This result matches the effect of the waveplate bandwidth described above. Our results show that the X-ray diagnostics for circular polarization lack full symmetry. This asymmetry arises from the off-center positioning of the polyethylene scatterer during X-ray irradiation[9].

The aforementioned experimental results demonstrate precise control over electron energy, with a wide range of radiation energy and polarization state. These verify the versatile multiparameter tunability of EPATCS. In our platform, the pulse duration of the electron bunch generated by LWFA is typically a few femtoseconds[47], and the laser pulse duration is 25 fs. Therefore, in order to realize the collision process described in Sections 3.2 and 3.3, following the approaches outlined in previous works[48,49], we implemented spatial and temporal synchronization, achieved measured time jitters below 10 fs and maintain a high spatial accuracy of electron-photon collisions within 5 μm. Moreover, our experimental results confirm that this level of precision is essential for stable electron–laser collisions.

4. A prospective roadmap for SF-QED research via EPATCS

By integrating with multi-PW laser facilities, the adjustable parameters of the EPATCS provide a fundamental platform for the approaching research initiatives, including multiphoton Thomson/Compton scattering, radiation reaction, vacuum polarization effects, and pair production[45,50–55]. When high-energy electrons interact with an intense laser, and the laser intensity in the rest frame of the electron approaches or reaches the Schwinger critical field $E_s = m_e^2 c^3/e\hbar$, the relativistic and nonlinear effects of the electrons in the electric field become significant. To describe such quantum effects, the quantum nonlinearity parameter $\chi_e = \sqrt{(F^{\mu\nu}p_\mu)^2}/(E_s m_e c)$ is defined, where $F^{\mu\nu} = \partial_\mu A_\nu - \partial_\nu A_\mu$, is the four-tensor electromagnetic field, p_μ represents the particle's four-momentum. When $\chi_e \ll 1$, classical electrodynamics can effectively describe the interaction between particles and electromagnetic fields. When $\chi_e \gtrsim 1$, quantum effects (such as electron-positron pair production and nonlinear Compton scattering) become significant, and classical theories are no longer applicable.

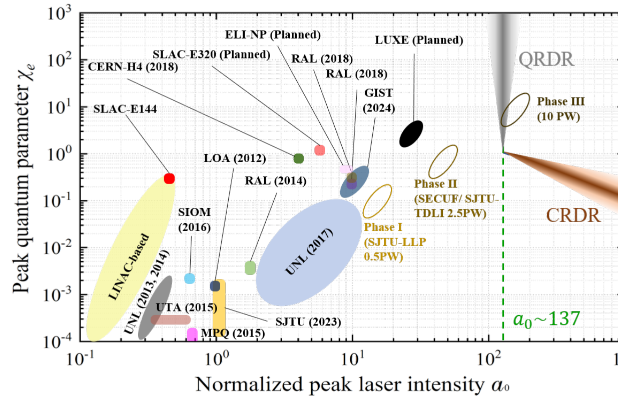

Figure 6. The relevant international experimental progress and proposals[3–6,11–17,56–65]. The solid-colored sections represent experiments that have been completed or are currently under planning, while the hollow elliptical regions correspond to the parameter ranges associated with the three phases discussed in this paper. The ranges corresponding to the classical radiation-dominated regime (CRDR) and the quantum radiation-dominated regime (QRDR) are indicated.

We plan to go through a three-phase development process to explore the SF-QED process through EPATCS. The table below presents the fundamental experimental proposal and parameters.

In phase I, the EPATCS will be transferred and built in multiple advanced laser facilities. The platform will be transferred to the 0.5 PW femtosecond laser facility, which is commissioned in the Key Laboratory of Laser Plasma at Shanghai Jiao Tong University. According to the matching condition of the laser wakefield acceleration, a low-energy dispersive electron beam with a maximum energy of less than 1 GeV can be generated stably. Another focused laser beam with an intensity up to $10^{21}\mathrm{W}\cdot\mathrm{cm}^{-2}$, corresponds to a normalized intensity of $a_0 \sim 20$. Under this premise, the quantum parameter is $\chi_e \sim 0.2$. In this regime, electrons interacting with an intense laser field undergo nonlinear Compton scattering, with multiphoton scattering emerging as a significant characteristic. The emission of high-energy radiation results in significant energy loss for the electrons. Future scientific exploration based on this platform will focus on investigating radiation reaction effects, nonlinear Compton scattering, etc.

In phase II, the platform will be transferred to the PW-level laser facilities, for instance, on a 1 PW laser facility at the Synergetic Extreme Condition User Facility (SECUF) of the Institute of Physics in the Chinese Academy of Sciences. It can contribute to research studies of the classical radiation-dominated regime (CRDR)[54,55] with normalized amplitude $a_0 \sim 40$. It can also be transferred to a 2.5 PW Ti: Sapphire femtosecond laser system in Tsung-Dao Lee Institute (TDLI), with a normalized amplitude a_0 can be up to 60. Meanwhile, a high-quality electron beam

https://doi.org/10.1017/hpl.2025.36 Published online by Cambridge University Press

Table 1. The fundamental experimental proposal and parameters

	Fundamental experimental proposal	Electron energy γ	Normalized intensity a_0	Quantum parameter χ_e
Phase I	From linear to nonlinear regime of ICS; Precision experiment of radiation reaction	$\lesssim 2000$	20	$\lesssim 0.2$
Phase II	Research studies of CRDR for Compton scattering	~ 4000	$40 \sim 60$	~ 1
Phase III	Research studies of QRDR for Compton scattering and BW process	$\gtrsim 4000$	~ 200	$\gtrsim 4$

with a central energy of 2 GeV, corresponding to $\gamma \approx 4000$, can be generated using an intense PW laser. At this point, the quantum parameter is $\chi_e \sim 1.4$, which allows the radiation reaction phenomenon to be observed more directly. Independently, high-precision spatiotemporal synchronization of EPATCS is crucial to validate and explore the locally monochromatic approximation (LMA)[66] and the local-constant-field approximation (LCFA)[67–71]. As the phenomenon becomes more pronounced, it would deepen our understanding of the fundamental principle of SF-QED.

In phase III, the EPATCS could be transferred to the 10 PW laser facilities, such as SULF[72], SEL[73], APOLLON[74], ELI[75,76] and EP-OPAL[77]. Consider that a stable electron energy of multi-GeV could be generated, the normalized amplitude a_0 of the scattering laser would be up to 200, when the laser beam is focused to the diffraction limit, and the quantum parameter could be higher than 4. When $a_0 \gtrsim 137$, and $\chi_e \gtrsim 1$, the radiation reaction in each photon emission is generally substantial and is fully accounted for within the context of SF-QED[78,79]. Under such conditions, quantum effects will become consequential, which will be conducive to researching the experimental phenomena in the quantum radiation dominant regime (QRDR)[54,79,80]. Furthermore, in this scenario, when the electron collides with the laser, the resulting high-energy gamma photons interact again with the intense laser. This interaction allows for effective detection of pair production, providing experimental evidence for the nonlinear Breit-Wheeler process[29,31]. This will deepen our understanding of SF-QED processes and further refine the SF-QED theories and experimental validation. The relevant international experimental progress and proposals are summarized as shown in Figure 6.

5. Conclusions

The development of an all-optical Thomson/Compton scattering platform, EPATCS, featuring versatile parameter tunability, harnesses the exceptional benefits of laser wakefield acceleration and superintense ultrafast lasers. We successfully demonstrate the capability of EPATCS by providing precise control over the parameters of the X-rays of ICS, including the energy spectrum, polarization state, and other parameters of high-energy radiation. With the ongoing development of super-intense ultrafast laser facilities, we aim to explore SF-QED in depth under various physical regimes, including radiation damping, nonlinear Compton scattering, and nonlinear Breit-Wheeler electron-positron pair production.

Appendix A. Principle of X/gamma-ray spectrum diagnostics

Due to differences in X-ray energy resulting from collisions at different angles, two diagnostic approaches are implemented.

In the ICS experiment with a collision angle of 30°, the X-ray energy range of 10 – 100 keV can be predicted based on Eq. (1) in the text and the electron spectrum. Within this energy range, the sector-shaped Ross-Filter was utilized for spectral diagnostics[81]. The corresponding reference formula is as follows:

$$S_k - S_{k+1} = \int d(E)[T_k(E) - T_{k+1}(E)]R(E)\frac{dN}{dE} \quad \text{(S1)}$$

Where S_k $(k = 1, 2, 3, \ldots)$ represent the signal intensity on the imaging plate after X-rays pass through metal filters of different types and thicknesses, T_k $(k = 1, 2, 3, \ldots)$ denote transmission of the filters for X-rays, $R(E)$ indicates the response efficiency of the imaging plate to X-rays at different energy levels, and dN/dE describes the final X-ray energy spectrum.

The signal distribution on the image plate behind the filters is shown in Figure S1 (a), and the transmission rate subtractions between adjacent filters are shown in Figure S1 (b). In the spectral deconvolution calculation, we assume that dN/dE is an independent value within each energy interval, thus simplifying the formula S1 to:

$$\frac{dN}{dE} = \frac{\int d(E)[T_k(E) - T_{k+1}(E)]R(E)}{S_k - S_{k+1}} \quad \text{(S2)}$$

By calculation dN/dE for different intervals and selecting the midpoint of each interval as the corresponding energy value, the spectrum curve of X-rays can be obtained. The horizontal error originates from the actual range of each energy interval, while the vertical error arises from the intensity fluctuations in the extracted signal region and the measurement error of the image plate response curve[82].

When the collision angle is 135°, the calculated gamma-

https://doi.org/10.1017/hpl.2025.36 Published online by Cambridge University Press

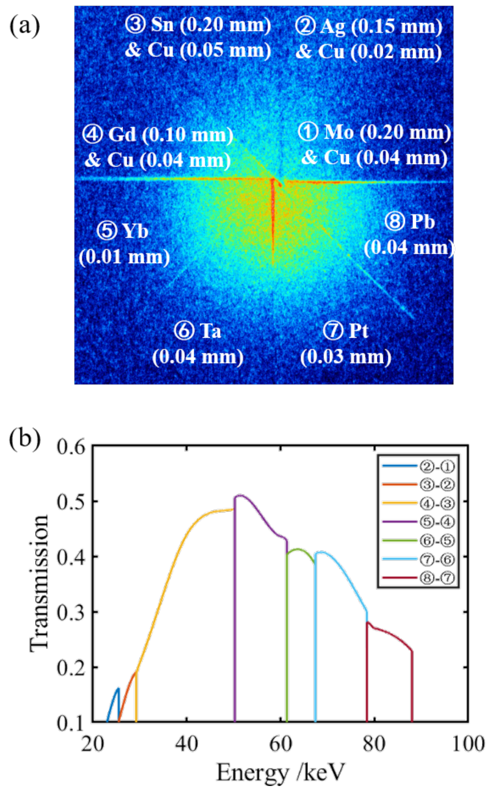

Figure S1. (a) The signal intensity distribution on the image plate in the 30° collision angle ICS experment, along with the corresponding types of metal filters and their respective thicknesses. (b) The transmission curves for different energy intervals are obtained by subtracting the transmission rates of adjacent filter combinations, where the annotated numbers correspond to the numbers in (a).

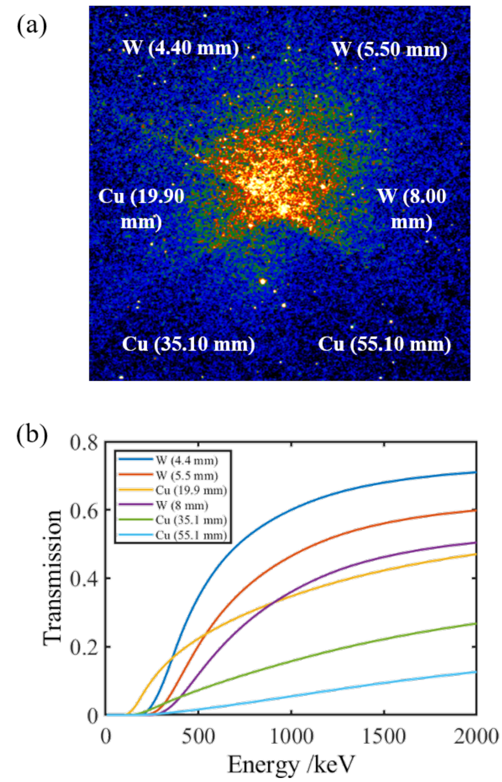

Figure S2. (a) The signal intensity distribution on the image plate in the 135° collision angle ICS experment, along with the corresponding types of metal filters and their respective thicknesses. (b) The radiation transmittance curves of different metal filters varying with energy.

ray spectrum extends to the MeV range. Within this energy range, the metal thickness required for gamma-ray absorption is mostly in the millimeter scale, and the corresponding distribution of gamma-ray transmission rate is shown in figure S2 (b). To solve the gamma-ray spectrum in this energy range, we employed an iterative fitting method based on underdetermined equations using the least squares approach.

Based on the electron spectrum, a corresponding gamma-ray spectrum can be calculated as a reference spectrum. Within the energy range of the reference spectrum, the gamma-ray reference spectra are discretized by selecting evenly spaced energy reference points E_j ($j = 1, 2, 3, \ldots, n$). The number of photons corresponding to each energy point is defined as N_j. Let the number of metal filters be m ($m < n$), and use this distribution as the reference spectrum type to substitute it into the gamma-ray transmission curve T_{ij}. The gamma-ray intensity distribution $S_i = \sum_j T_{ij} N_j$ is then obtained under different thicknesses and materials. Meanwhile, the experimentally measured intensity distribution is r_i ($i = 1, 2, 3, \ldots, m$), as shown in Figure S2 (a). Considering the relatively low response efficiency of the image plate to MeV gamma-rays, CsI crystals are used here to diagnose the energy deposition distribution of gamma-rays (where the response of CsI to gamma-rays of different energies is R_{ij}). For simplicity, we define $T'_{ij} = T_{ij} R_{ij}$. Following this, the evaluation function is defined as the variance between the signal intensity derived from the reference spectrum and the measured signal.

$$\sigma = \sum_i (r_i - S_i)^2 \tag{S3}$$

With this evaluation function, multiple iterative calculations are performed and the iterative function is as follows[3]:

$$N'_j = N_j + \frac{\alpha \sum_i (T'_{ij} \times \frac{r_i - S_i}{\sum_k T'_{ik}})}{\sum_k T'_{kj}} \tag{S4}$$

Iteration proceeds until the variance minimizes, at which point the process concludes, yielding the final radiation spectrum. The errors mainly arise from the numerical fluctuations in signal intensity across various regions of the experimental results.

https://doi.org/10.1017/hpl.2025.36 Published online by Cambridge University Press

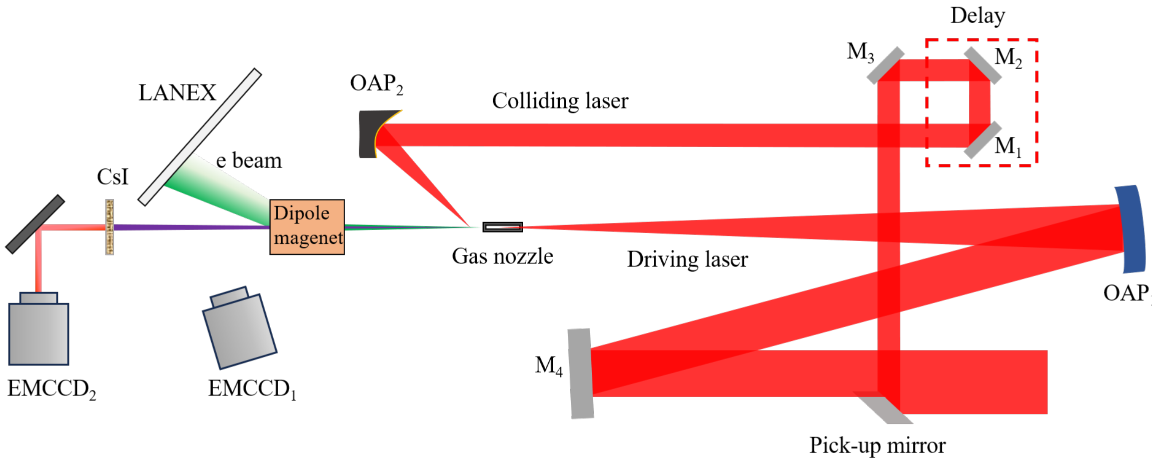

Figure S3. The overlap geometry of the experimental schematic diagram.

Appendix B. The experimental schematic diagram.

The primary components of the experiment include two laser beams, a gas nozzle, and diagnostic systems for both electrons and radiation, as shown in Figure S3. A portion of the laser beam from the main optical path is extracted using a pick-up mirror to serve as the collision laser, while the remaining portion is focused by an F#20 long-focus off-axis parabolic (OAP) mirror onto a gas nozzle. After passing through a delay line, the collision laser is focused by an F#5 OAP mirror to a point 1 mm downstream of the nozzle. After scattering, electrons are deflected by a dipole magnet to measure the electron energy spectrum, and the emitted radiation hits a CsI scintillator to produce fluorescence, which is used to observe the profile of high-energy gamma radiation.

For energy spectrum measurements, filters are added between the magnet and CsI to perform radiation spectrum diagnostics. When the radiation energy is on the order of tens of keV or lower, an image plate is used instead of the CsI scintillator to image the radiation profile. For polarization measurements, a cylindrical plastic converter is placed after the electron deflection, along with four image plates positioned perpendicular to each other.

Acknowledgements

This work is supported by the National Key R&D Program of China (2021YFA1601700), the National Natural Science Foundation of China (12074251, 11991073, 12335016, 12105174, 12225505) and the Strategic Priority Research Program of the Chinese Academy of Sciences (Grant No. XDA25030400, XDA25010100). The authors would like to acknowledge the sponsorship from the Yangyang Development Fund. The authors thank Songyu Ge and Rongzhao Hu from Shanghai Run Li Vacuum Technology Co., Ltd.

References

1. Julian Schwinger. On Gauge Invariance and Vacuum Polarization. *Physical Review*, 82(5):664–679, June 1951. ISSN 0031-899X. doi: 10.1103/PhysRev.82.664. URL https://link.aps.org/doi/10.1103/PhysRev.82.664.
2. T. Tajima and J. M. Dawson. Laser Electron Accelerator. *Physical Review Letters*, 43(4):267–270, July 1979. ISSN 0031-9007. doi: 10.1103/PhysRevLett.43.267. URL https://link.aps.org/doi/10.1103/PhysRevLett.43.267.
3. K. Ta Phuoc, S. Corde, C. Thaury, V. Malka, A. Tafzi, J. P. Goddet, R. C. Shah, S. Sebban, and A. Rousse. All-optical Compton gamma-ray source. *Nature Photonics*, 6(5):308–311, May 2012. ISSN 1749-4885, 1749-4893. doi: 10.1038/nphoton.2012.82. URL https://www.nature.com/articles/nphoton.2012.82.
4. Hai-En Tsai, Xiaoming Wang, Joseph M. Shaw, Zhengyan Li, Alexey V. Arefiev, Xi Zhang, Rafal Zgadzaj, Watson Henderson, V. Khudik, G. Shvets, and M. C. Downer. Compact tunable Compton x-ray source from laser-plasma accelerator and plasma mirror. *Physics of Plasmas*, 22 (2):023106, February 2015. ISSN 1070-664X, 1089-7674. doi: 10.1063/1.4907655. URL https://pubs.aip.org/pop/article/22/2/023106/109840/Compact-tunable-Compton-x-ray-source-from-laser.
5. Changhai Yu, Rong Qi, Wentao Wang, Jiansheng Liu, Wentao Li, Cheng Wang, Zhijun Zhang, Jiaqi Liu, Zhiyong Qin, Ming Fang, Ke Feng, Ying Wu, Ye Tian, Yi Xu, Fenxiang Wu, Yuxin Leng, Xiufeng Weng, Jihu Wang, Fuli Wei, Yicheng Yi, Zhaohui Song, Ruxin Li, and Zhizhan Xu. Ultrahigh brilliance quasi-monochromatic MeV γ-rays based on self-synchronized all-optical Compton scattering. *Scientific Reports*, 6 (1):29518, July 2016. ISSN 2045-2322. doi: 10.

1038/srep29518. URL https://www.nature.com/articles/srep29518.

6. A Döpp, E Guillaume, C Thaury, J Gautier, I Andriyash, A Lifschitz, V Malka, A Rousse, and K Ta Phuoc. An all-optical Compton source for single-exposure x-ray imaging. *Plasma Physics and Controlled Fusion*, 58(3):034005, March 2016. ISSN 0741-3335, 1361-6587. doi: 10.1088/0741-3335/58/3/034005. URL https://iopscience.iop.org/article/10.1088/0741-3335/58/3/034005.
7. Changqing Zhu, Jinguang Wang, Jie Feng, Yifei Li, Dazhang Li, Minghua Li, Yuhang He, Jinglong Ma, Junhao Tan, Baolong Zhang, Wenchao Yan, and Liming Chen. Inverse Compton scattering x-ray source from laser electron accelerator in pure nitrogen with 15 TW laser pulses. *Plasma Physics and Controlled Fusion*, 61(2):024001, February 2019. ISSN 0741-3335, 1361-6587. doi: 10.1088/1361-6587/aaebe3. URL https://iopscience.iop.org/article/10.1088/1361-6587/aaebe3.
8. Ying Wu, Changhai Yu , Zhiyong Qin, Wentao Wang, Rong Qi,, Zhijun Zhang, Ke Feng, Lintong Ke, Yu Chen, Cheng Wang,, and Jiansheng Liu, Ruxin Li and Zhizhan Xu,. Dual-color γ-rays via all-optical Compton scattering from a cascaded laser-driven wakefield accelerator. *Plasma Phys. Control. Fusion*, 61 (085030), 2019.
9. Yue Ma, Jianfei Hua, Dexiang Liu, Yunxiao He, Tianliang Zhang, Jiucheng Chen, Fan Yang, Xiaonan Ning, Hongze Zhang, Yingchao Du, and Wei Lu. Compact Polarized X-Ray Source Based on All-Optical Inverse Compton Scattering. *Physical Review Applied*, 19(1):014073, January 2023. ISSN 2331-7019. doi: 10.1103/PhysRevApplied.19.014073. URL https://link.aps.org/doi/10.1103/PhysRevApplied.19.014073.
10. Yan-Jun Gu and Stefan Weber. Intense, directional and tunable γ-ray emission via relativistic oscillating plasma mirror. *Optics Express*, 26(16):19932, August 2018. ISSN 1094-4087. doi: 10.1364/OE.26.019932. URL https://opg.optica.org/abstract.cfm?URI=oe-26-16-19932.
11. J.M. Cole, K.T. Behm, E. Gerstmayr, T.G. Blackburn, J.C. Wood, C.D. Baird, M.J. Duff, C. Harvey, A. Ilderton, A.S. Joglekar, K. Krushelnick, S. Kuschel, M. Marklund, P. McKenna, C.D. Murphy, K. Poder, C.P. Ridgers, G.M. Samarin, G. Sarri, D.R. Symes, A.G.R. Thomas, J. Warwick, M. Zepf, Z. Najmudin, and S.P.D. Mangles. Experimental Evidence of Radiation Reaction in the Collision of a High-Intensity Laser Pulse with a Laser-Wakefield Accelerated Electron Beam. *Physical Review X*, 8(1):011020, February 2018. ISSN 2160-3308. doi: 10.1103/PhysRevX.8.011020. URL https://link.aps.org/doi/10.1103/PhysRevX.8.011020.
12. K. Poder, M. Tamburini, G. Sarri, A. Di Piazza, S. Kuschel, C.D. Baird, K. Behm, S. Bohlen, J.M. Cole, D.J. Corvan, M. Duff, E. Gerstmayr, C.H. Keitel, K. Krushelnick, S.P.D. Mangles, P. McKenna, C.D. Murphy, Z. Najmudin, C.P. Ridgers, G.M. Samarin, D.R. Symes, A.G.R. Thomas, J. Warwick, and M. Zepf. Experimental Signatures of the Quantum Nature of Radiation Reaction in the Field of an Ultraintense Laser. *Physical Review X*, 8(3):031004, July 2018. ISSN 2160-3308. doi: 10.1103/PhysRevX.8.031004. URL https://link.aps.org/doi/10.1103/PhysRevX.8.031004.
13. N. D. Powers, I. Ghebregziabher, G. Golovin, C. Liu, S. Chen, S. Banerjee, J. Zhang, and D. P. Umstadter. Quasi-monoenergetic and tunable X-rays from a laser-driven Compton light source. *Nature Photonics*, 8(1): 28–31, January 2014. ISSN 1749-4885, 1749-4893. doi: 10.1038/nphoton.2013.314. URL https://www.nature.com/articles/nphoton.2013.314.
14. S. Chen, N. D. Powers, I. Ghebregziabher, C. M. Maharjan, C. Liu, G. Golovin, S. Banerjee, J. Zhang, N. Cunningham, A. Moorti, S. Clarke, S. Pozzi, and D. P. Umstadter. MeV-Energy Rays from Inverse Compton Scattering with Laser-Wakefield Accelerated Electrons. *Physical Review Letters*, 110(15):155003, April 2013. ISSN 0031-9007, 1079-7114. doi: 10.1103/PhysRevLett.110.155003. URL https://link.aps.org/doi/10.1103/PhysRevLett.110.155003.
15. Cheng Liu, Grigory Golovin, Shouyuan Chen, Jun Zhang, Baozhen Zhao, Daniel Haden, Sudeep Banerjee, Jack Silano, Hugon Karwowski, and Donald Umstadter. Generation of 9 MeV γ-rays by all-laser-driven Compton scattering with second-harmonic laser light. *Optics Letters*, 39(14):4132, July 2014. ISSN 0146-9592, 1539-4794. doi: 10.1364/OL.39.004132. URL https://opg.optica.org/abstract.cfm?URI=ol-39-14-4132.
16. K. Khrennikov, J. Wenz, A. Buck, J. Xu, M. Heigoldt, L. Veisz, and S. Karsch. Tunable All-Optical Quasimonochromatic Thomson X-Ray Source in the Nonlinear Regime. *Physical Review Letters*, 114(19): 195003, May 2015. ISSN 0031-9007, 1079-7114. doi: 10.1103/PhysRevLett.114.195003. URL https://link.aps.org/doi/10.1103/PhysRevLett.114.195003.
17. Wenchao Yan, Colton Fruhling, Grigory Golovin, Daniel Haden, Ji Luo, Ping Zhang, Baozhen Zhao, Jun Zhang, Cheng Liu, Min Chen, Shouyuan Chen, Sudeep Banerjee, and Donald Umstadter. High-order multiphoton Thomson scattering. *Nature Photonics*, 11 (8):514–520, August 2017. ISSN 1749-4885, 1749-4893. doi: 10.1038/nphoton.2017.100. URL https://www.nature.com/articles/nphoton.2017.100.
18. A. Pukhov and J. Meyer-ter Vehn. Laser wake field acceleration: the highly non-linear broken-wave regime. *Applied Physics B: Lasers and Optics*, 74(4-5):355–361, April 2002. ISSN 0946-2171, 1432-0649. doi: 10.1007/s003400200795. URL http://link.springer.com/10.1007/s003400200795.

19. L. B. Fletcher, H. J. Lee, T. Döppner, E. Galtier, B. Nagler, P. Heimann, C. Fortmann, S. LePape, T. Ma, M. Millot, A. Pak, D. Turnbull, D. A. Chapman, D. O. Gericke, J. Vorberger, T. White, G. Gregori, M. Wei, B. Barbrel, R. W. Falcone, C.-C. Kao, H. Nuhn, J. Welch, U. Zastrau, P. Neumayer, J. B. Hastings, and S. H. Glenzer. Ultrabright X-ray laser scattering for dynamic warm dense matter physics. *Nature Photonics*, 9(4):274–279, April 2015. ISSN 1749-4885, 1749-4893. doi: 10.1038/nphoton.2015.41. URL https://www.nature.com/articles/nphoton.2015.41.

20. Tais Gorkhover, Sebastian Schorb, Ryan Coffee, Marcus Adolph, Lutz Foucar, Daniela Rupp, Andrew Aquila, John D. Bozek, Sascha W. Epp, Benjamin Erk, Lars Gumprecht, Lotte Holmegaard, Andreas Hartmann, Robert Hartmann, Günter Hauser, Peter Holl, Andre Hömke, Per Johnsson, Nils Kimmel, Kai-Uwe Kühnel, Marc Messerschmidt, Christian Reich, Arnaud Rouzée, Benedikt Rudek, Carlo Schmidt, Joachim Schulz, Heike Soltau, Stephan Stern, Georg Weidenspointner, Bill White, Jochen Küpper, Lothar Strüder, Ilme Schlichting, Joachim Ullrich, Daniel Rolles, Artem Rudenko, Thomas Möller, and Christoph Bostedt. Femtosecond and nanometre visualization of structural dynamics in superheated nanoparticles. *Nature Photonics*, 10(2):93–97, February 2016. ISSN 1749-4885, 1749-4893. doi: 10.1038/nphoton.2015.264. URL https://www.nature.com/articles/nphoton.2015.264.

21. Andreas Schropp, Robert Hoppe, Vivienne Meier, Jens Patommel, Frank Seiboth, Yuan Ping, Damien G. Hicks, Martha A. Beckwith, Gilbert W. Collins, Andrew Higginbotham, Justin S. Wark, Hae Ja Lee, Bob Nagler, Eric C. Galtier, Brice Arnold, Ulf Zastrau, Jerome B. Hastings, and Christian G. Schroer. Imaging Shock Waves in Diamond with Both High Temporal and Spatial Resolution at an XFEL. *Scientific Reports*, 5(1):11089, June 2015. ISSN 2045-2322. doi: 10.1038/srep11089. URL https://www.nature.com/articles/srep11089.

22. T. Kluge, C. Rödel, M. Rödel, A. Pelka, E. E. McBride, L. B. Fletcher, M. Harmand, A. Krygier, A. Higginbotham, M. Bussmann, E. Galtier, E. Gamboa, A. L. Garcia, M. Garten, S. H. Glenzer, E. Granados, C. Gutt, H. J. Lee, B. Nagler, W. Schumaker, F. Tavella, M. Zacharias, U. Schramm, and T. E. Cowan. Nanometer-scale characterization of laser-driven compression, shocks, and phase transitions, by x-ray scattering using free electron lasers. *Physics of Plasmas*, 24(10):102709, October 2017. ISSN 1070-664X, 1089-7674. doi: 10.1063/1.5008289. URL https://pubs.aip.org/pop/article/24/10/102709/795195/Nanometer-scale-characterization-of-laser-driven.

23. Thomas Kluge, Melanie Rödel, Josefine Metzkes-Ng, Alexander Pelka, Alejandro Laso Garcia, Irene Prencipe, Martin Rehwald, Motoaki Nakatsutsumi, Emma E. McBride, Tommy Schönherr, Marco Garten, Nicholas J. Hartley, Malte Zacharias, Jörg Grenzer, Artur Erbe, Yordan M. Georgiev, Eric Galtier, Inhyuk Nam, Hae Ja Lee, Siegfried Glenzer, Michael Bussmann, Christian Gutt, Karl Zeil, Christian Rödel, Uwe Hübner, Ulrich Schramm, and Thomas E. Cowan. Observation of Ultrafast Solid-Density Plasma Dynamics Using Femtosecond X-Ray Pulses from a Free-Electron Laser. *Physical Review X*, 8(3):031068, September 2018. ISSN 2160-3308. doi: 10.1103/PhysRevX.8.031068. URL https://link.aps.org/doi/10.1103/PhysRevX.8.031068.

24. Mianzhen Mo, Samuel Murphy, Zhijiang Chen, Paul Fossati, Renkai Li, Yongqiang Wang, Xijie Wang, and Siegfried Glenzer. Visualization of ultrafast melting initiated from radiation-driven defects in solids. *Science Advances*, 5(5):eaaw0392, May 2019. ISSN 2375-2548. doi: 10.1126/sciadv.aaw0392. URL https://www.science.org/doi/10.1126/sciadv.aaw0392.

25. Lennart Gaus, Lothar Bischoff, Michael Bussmann, Eric Cunningham, Chandra B. Curry, Juncheng E, Eric Galtier, Maxence Gauthier, Alejandro Laso García, Marco Garten, Siegfried Glenzer, Jörg Grenzer, Christian Gutt, Nicholas J. Hartley, Lingen Huang, Uwe Hübner, Dominik Kraus, Hae Ja Lee, Emma E. McBride, Josefine Metzkes-Ng, Bob Nagler, Motoaki Nakatsutsumi, Jan Nikl, Masato Ota, Alexander Pelka, Irene Prencipe, Lisa Randolph, Melanie Rödel, Youichi Sakawa, Hans-Peter Schlenvoigt, Michal Šmíd, Franziska Treffert, Katja Voigt, Karl Zeil, Thomas E. Cowan, Ulrich Schramm, and Thomas Kluge. Probing ultrafast laser plasma processes inside solids with resonant small-angle x-ray scattering. *Physical Review Research*, 3(4):043194, December 2021. ISSN 2643-1564. doi: 10.1103/PhysRevResearch.3.043194. URL https://link.aps.org/doi/10.1103/PhysRevResearch.3.043194.

26. Yuchi Wu, Shaoyi Wang, Bin Zhu, Yonghong Yan, Minghai Yu, Gang Li, Xiaohui Zhang, Yue Yang, Fang Tan, Feng Lu, Bi Bi, Xiaoqin Mao, Zhonghai Wang, Zongqing Zhao, Jingqin Su, Weimin Zhou, and Yuqiu Gu. Virtual source approach for maximizing resolution in high-penetration gamma-ray imaging. *Matter and Radiation at Extremes*, 9(3):037202, May 2024. ISSN 2468-2047, 2468-080X. doi: 10.1063/5.0179781. URL https://pubs.aip.org/mre/article/9/3/037202/3272575/Virtual-source-approach-for-maximizing-resolution.

27. D. Habs, T. Tajima, J. Schreiber, C. P.J. Barty, M. Fujiwara, and P. G. Thirolf. Vision of nuclear physics with photo-nuclear reactions by laser-driven $\sf \gamma$ beams. *The European Physical Journal D*, 55(2):279–285, November 2009. ISSN 1434-6060, 1434-6079. doi: 10.1140/epjd/e2009-00101-2. URL

http://link.springer.com/10.1140/epjd/e2009-00101-2.

28. Hans A. Weidenmüller. Nuclear Excitation by a Zeptosecond Multi-MeV Laser Pulse. *Physical Review Letters*, 106(12):122502, March 2011. ISSN 0031-9007, 1079-7114. doi: 10.1103/PhysRevLett.106.122502. URL https://link.aps.org/doi/10.1103/PhysRevLett.106.122502.
29. G. Breit and John A. Wheeler. Collision of Two Light Quanta. *Physical Review*, 46(12):1087–1091, December 1934. ISSN 0031-899X. doi: 10.1103/PhysRev.46.1087. URL https://link.aps.org/doi/10.1103/PhysRev.46.1087.
30. Howard R. Reiss. Absorption of Light by Light. *Journal of Mathematical Physics*, 3(1):59–67, January 1962. ISSN 0022-2488, 1089-7658. doi: 10.1063/1.1703787. URL https://pubs.aip.org/jmp/article/3/1/59/453781/Absorption-of-Light-by-Light.
31. Yan-Jun Gu, Ondrej Klimo, Sergei V. Bulanov, and Stefan Weber. Brilliant gamma-ray beam and electron–positron pair production by enhanced attosecond pulses. *Communications Physics*, 1(1):93, December 2018. ISSN 2399-3650. doi: 10.1038/s42005-018-0095-3. URL https://www.nature.com/articles/s42005-018-0095-3.
32. V. Petrillo, G. Dattoli, I. Drebot, and F. Nguyen. Compton Scattered X-Gamma Rays with Orbital Momentum. *Physical Review Letters*, 117(12):123903, September 2016. ISSN 0031-9007, 1079-7114. doi: 10.1103/PhysRevLett.117.123903. URL https://link.aps.org/doi/10.1103/PhysRevLett.117.123903.
33. Yue-Yue Chen, Jian-Xing Li, Karen Z. Hatsagortsyan, and Christoph H. Keitel. γ -Ray Beams with Large Orbital Angular Momentum via Nonlinear Compton Scattering with Radiation Reaction. *Physical Review Letters*, 121(7):074801, August 2018. ISSN 0031-9007, 1079-7114. doi: 10.1103/PhysRevLett.121.074801. URL https://link.aps.org/doi/10.1103/PhysRevLett.121.074801.
34. Mamutjan Ababekri, Ren-Tong Guo, Feng Wan, B. Qiao, Zhongpeng Li, Chong Lv, Bo Zhang, Weimin Zhou, Yuqiu Gu, and Jian-Xing Li. Vortex γ photon generation via spin-to-orbital angular momentum transfer in nonlinear Compton scattering. *Physical Review D*, 109(1):016005, January 2024. ISSN 2470-0010, 2470-0029. doi: 10.1103/PhysRevD.109.016005. URL https://link.aps.org/doi/10.1103/PhysRevD.109.016005.
35. Andreas Döpp, Kim Ta Phuoc, and Igor A. Andriyash. All-optical Compton scattering at shallow interaction angles. *Journal of Plasma Physics*, 89 (5):965890501, October 2023. ISSN 0022-3778, 1469-7807. doi: 10.1017/S0022377823000909. URL https://www.cambridge.org/core/product/identifier/S0022377823000909/type/journal_article.
36. Weijun Zhou, Wenchao Yan, Jinguang Wang, and Liming Chen. Gamma-ray Vortex Burst in Nonlinear Thomson Scattering with Refocusing Spiral Plasma Mirror. *Ultrafast Science*, 3:0005, January 2023. ISSN 2097-0331, 2765-8791. doi: 10.34133/ultrafastscience.0005. URL https://spj.science.org/doi/10.34133/ultrafastscience.0005.
37. A. Debus, S. Bock, M. Bussmann, T. E. Cowan, A. Jochmann, T. Kluge, S. D. Kraft, R. Sauerbrey, K. Zeil, and U. Schramm. Linear and non-linear Thomson-scattering x-ray sources driven by conventionally and laser plasma accelerated electrons. page 735908, Prague, Czech Republic, May 2009. doi: 10.1117/12.820741. URL http://proceedings.spiedigitallibrary.org/proceeding.aspx?doi=10.1117/12.820741.
38. J. Wenz, A. Döpp, K. Khrennikov, S. Schindler, M. F. Gilljohann, H. Ding, J. Götzfried, A. Buck, J. Xu, M. Heigoldt, W. Helml, L. Veisz, and S. Karsch. Dual-energy electron beams from a compact laser-driven accelerator. *Nature Photonics*, 13(4):263–269, April 2019. ISSN 1749-4885, 1749-4893. doi: 10.1038/s41566-019-0356-z. URL https://www.nature.com/articles/s41566-019-0356-z.
39. Pin-Hua Huang, Kenneth R. Kase, and Bengt E. Bjärngard. Simulation studies of 4-MV x-ray spectral reconstruction by numerical analysis of transmission data. *Medical Physics*, 9(5):695–702, September 1982. ISSN 0094-2405, 2473-4209. doi: 10.1118/1.595131. URL https://aapm.onlinelibrary.wiley.com/doi/10.1118/1.595131.
40. Hiroyuki Ohsumi and Taka-hisa Arima. Novel insight into structural magnetism by polarized synchrotron X-ray scattering. *Advances in Physics: X*, 1(1):128–145, January 2016. ISSN 2374-6149. doi: 10.1080/23746149.2016.1150202. URL http://www.tandfonline.com/doi/full/10.1080/23746149.2016.1150202.
41. Yoshihiko Togawa, Yusuke Kousaka, Katsuya Inoue, and Jun-ichiro Kishine. Symmetry, Structure, and Dynamics of Monoaxial Chiral Magnets. *Journal of the Physical Society of Japan*, 85(11):112001, November 2016. ISSN 0031-9015, 1347-4073. doi: 10.7566/JPSJ.85.112001. URL http://journals.jps.jp/doi/10.7566/JPSJ.85.112001.
42. S. L. Zhang, G. Van Der Laan, and T. Hesjedal. Direct experimental determination of spiral spin structures via the dichroism extinction effect in resonant elastic soft x-ray scattering. *Physical Review B*, 96(9):094401, September 2017. ISSN 2469-9950, 2469-9969. doi: 10.1103/PhysRevB.96.094401. URL https://link.aps.org/doi/10.1103/PhysRevB.96.094401.
43. Annika T. Schmitt, Yves Joly, Kai S. Schulze, Berit Marx-Glowna, Ingo Uschmann, Benjamin Grabiger, Hendrik Bernhardt, Robert Loetzsch, Amélie Juhin, Jérôme Debray, Hans-Christian Wille, Hasan Yavaş,

Gerhard G. Paulus, and Ralf Röhlsberger. Disentangling x-ray dichroism and birefringence via high-purity polarimetry. *Optica*, 8(1):56, January 2021. ISSN 2334-2536. doi: 10.1364/OPTICA.410357. URL https://opg.optica.org/abstract.cfm?URI=optica-8-1-56.

44. D. P. Siddons, M. Hart, Y. Amemiya, and J. B. Hastings. X-ray optical activity and the Faraday effect in cobalt and its compounds. *Physical Review Letters*, 64(16):1967–1970, April 1990. ISSN 0031-9007. doi: 10.1103/PhysRevLett.64.1967. URL https://link.aps.org/doi/10.1103/PhysRevLett.64.1967.
45. Guang-Peng An, Yun-Long Chi, Yong-Le Dang, Guang-Yong Fu, Bing Guo, Yong-Sheng Huang, Chuang-Ye He, Xiang-Cheng Kong, Xiao-Fei Lan, Jia-Cai Li, Fu-Long Liu, Jin-Shui Shi, Xian-Jing Sun, Yi Wang, Jian-Li Wang, Lin Wang, Yuan-Yuan Wei, Gang Wu, Guang-Lei Xu, Xiao-Feng Xi, Guo-Jun Yang, Chun-Lei Zhang, Zhuo Zhang, Zhi-Peng Zheng, Xiao-Ding Zhang, and Shao-Ping Zhang. High energy and high brightness laser compton backscattering gamma-ray source at IHEP. *Matter and Radiation at Extremes*, 3(4):219–226, July 2018. ISSN 2468-2047, 2468-080X. doi: 10.1016/j.mre.2018.01.005. URL https://pubs.aip.org/mre/article/3/4/219/252898/High-energy-and-high-brightness-laser-compton.
46. Gerardo O. Depaola. New monte carlo method for compton and rayleigh scattering by polarized gamma rays. *Nuclear Instruments & Methods in Physics Research Section A-accelerators Spectrometers Detectors and Associated Equipment*, 512:619–630, 2003. URL https://api.semanticscholar.org/CorpusID:120334854.
47. Olle Lundh, J Lim, Clément Rechatin, L Ammoura, Ahmed Ben-Ismaïl, X Davoine, Guilhem Gallot, Jean-Philippe Goddet, E Lefebvre, Victor Malka, et al. Few femtosecond, few kiloampere electron bunch produced by a laser–plasma accelerator. *Nature Physics*, 7(3):219–222, 2011.
48. Do Yeon Kim, Calin Ioan Hojbota, Mohammad Mirzaie, Seong Ku Lee, Ki Yong Kim, Jae Hee Sung, and Chang Hee Nam. Optical synchronization technique for all-optical compton scattering. *Review of Scientific Instruments*, 93(11):113001, 11 2022. ISSN 0034-6748. doi: 10.1063/5.0115918. URL https://doi.org/10.1063/5.0115918.
49. D. J. Corvan, T. Dzelzainis, C. Hyland, G. Nersisyan, M. Yeung, M. Zepf, and G. Sarri. Optical measurement of the temporal delay between two ultra-short and focussed laser pluses. *Opt. Express*, 24(3):3127–3136, Feb 2016. doi: 10.1364/OE.24.003127. URL https://opg.optica.org/oe/abstract.cfm?URI=oe-24-3-3127.
50. A. Gonoskov, T.G. Blackburn, M. Marklund, and S.S. Bulanov. Charged particle motion and radiation in strong electromagnetic fields. *Reviews of Modern Physics*, 94(4):045001, October 2022. ISSN 0034-6861, 1539-0756. doi: 10.1103/RevModPhys.94.045001. URL https://link.aps.org/doi/10.1103/RevModPhys.94.045001.
51. A. Di Piazza, C. Müller, K. Z. Hatsagortsyan, and C. H. Keitel. Extremely high-intensity laser interactions with fundamental quantum systems. *Reviews of Modern Physics*, 84(3):1177–1228, August 2012. ISSN 0034-6861, 1539-0756. doi: 10.1103/RevModPhys.84.1177. URL https://link.aps.org/doi/10.1103/RevModPhys.84.1177.
52. S. Weber, S. Bechet, S. Borneis, L. Brabec, M. Bučka, E. Chacon-Golcher, M. Ciappina, M. DeMarco, A. Fajstavr, K. Falk, E.-R. Garcia, J. Grosz, Y.-J. Gu, J.-C. Hernandez, M. Holec, P. Janečka, M. Jantač, M. Jirka, H. Kadlecova, D. Khikhlukha, O. Klimo, G. Korn, D. Kramer, D. Kumar, T. Lastovička, P. Lutoslawski, L. Morejon, V. Olšovcová, M. Rajdl, O. Renner, B. Rus, S. Singh, M. Šmid, M. Sokol, R. Versaci, R. Vrána, M. Vranic, J. Vyskočil, A. Wolf, and Q. Yu. P3: An installation for high-energy density plasma physics and ultra-high intensity laser–matter interaction at ELI-Beamlines. *Matter and Radiation at Extremes*, 2(4):149–176, July 2017. ISSN 2468-2047, 2468-080X. doi: 10.1016/j.mre.2017.03.003. URL https://pubs.aip.org/mre/article/2/4/149/252778/P3-An-installation-for-high-energy-density-plasma.
53. Yan-Jun Gu, Martin Jirka, Ondrej Klimo, and Stefan Weber. Gamma photons and electron-positron pairs from ultra-intense laser-matter interaction: A comparative study of proposed configurations. *Matter and Radiation at Extremes*, 4(6):064403, November 2019. ISSN 2468-2047, 2468-080X. doi: 10.1063/1.5098978. URL https://pubs.aip.org/mre/article/4/6/064403/253056/Gamma-photons-and-electron-positron-pairs-from.
54. A. S. Samsonov, E. N. Nerush, and I. Yu. Kostyukov. High-order corrections to the radiation-free dynamics of an electron in the strongly radiation-dominated regime. *Matter and Radiation at Extremes*, 8 (1):014402, January 2023. ISSN 2468-2047, 2468-080X. doi: 10.1063/5.0117504. URL https://pubs.aip.org/mre/article/8/1/014402/2874869/High-order-corrections-to-the-radiation-free.
55. S. S. Bulanov, C. B. Schroeder, E. Esarey, and W. P. Leemans. Electromagnetic cascade in high-energy electron, positron, and photon interactions with intense laser pulses. *Physical Review A*, 87(6):062110, June 2013. ISSN 1050-2947, 1094-1622. doi: 10.1103/PhysRevA.87.062110. URL https://link.aps.org/doi/10.1103/PhysRevA.87.062110.
56. C. Bula, K. T. McDonald, E. J. Prebys, C. Bamber, S. Boege, T. Kotseroglou, A. C. Melissinos, D. D. Meyerhofer, W. Ragg, D. L. Burke, R. C. Field,

G. Horton-Smith, A. C. Odian, J. E. Spencer, D. Walz, S. C. Berridge, W. M. Bugg, K. Shmakov, and A. W. Weidemann. Observation of Nonlinear Effects in Compton Scattering. *Physical Review Letters*, 76(17): 3116–3119, April 1996. ISSN 0031-9007, 1079-7114. doi: 10.1103/PhysRevLett.76.3116. URL https://link.aps.org/doi/10.1103/PhysRevLett.76.3116.

57. D L Burke, R C Field, G Horton-Smith, J E Spencer, D Walz, S C Berridge, W M Bugg, K Shmakov, A W Weidemann, C Bula, K T McDonald, E J Prebys, C Bamber, S J Boege, T Koffas, T Kotseroglou, A C Melissinos, D D Meyerhofer, D A Reis, and W Ragg. Positron Production in Multiphoton Light-by-Light Scattering. *Physical Review Letters*, 79(9), 1997.

58. H. Schwoerer, B. Liesfeld, H.-P. Schlenvoigt, K.-U. Amthor, and R. Sauerbrey. Thomson-Backscattered X Rays From Laser-Accelerated Electrons. *Physical Review Letters*, 96(1):014802, January 2006. ISSN 0031-9007, 1079-7114. doi: 10.1103/PhysRevLett.96.014802. URL https://link.aps.org/doi/10.1103/PhysRevLett.96.014802.

59. G. Sarri, D.J. Corvan, W. Schumaker, J.M. Cole, A. Di Piazza, H. Ahmed, C. Harvey, C.H. Keitel, K. Krushelnick, S.P.D. Mangles, Z. Najmudin, D. Symes, A.G.R. Thomas, M. Yeung, Z. Zhao, and M. Zepf. Ultrahigh Brilliance Multi-MeV γ -Ray Beams from Nonlinear Relativistic Thomson Scattering. *Physical Review Letters*, 113(22):224801, November 2014. ISSN 0031-9007, 1079-7114. doi: 10.1103/PhysRevLett.113.224801. URL https://link.aps.org/doi/10.1103/PhysRevLett.113.224801.

60. Mohammad Mirzaie, Calin Ioan Hojbota, Do Yeon Kim, Vishwa Bandhu Pathak, Tae Gyu Pak, Chul Min Kim, Hwang Woon Lee, Jin Woo Yoon, Seong Ku Lee, Yong Joo Rhee, Marija Vranic, Óscar Amaro, Ki Yong Kim, Jae Hee Sung, and Chang Hee Nam. All-optical nonlinear Compton scattering performed with a multi-petawatt laser. *Nature Photonics*, 18(11):1212–1217, November 2024. ISSN 1749-4885, 1749-4893. doi: 10.1038/s41566-024-01550-8. URL https://www.nature.com/articles/s41566-024-01550-8.

61. I C E Turcu, F Negoita, D A Jaroszynski, P Mckenna, S Balascuta, D Ursescu, I Dancus, M O Cernaianu, M V Tataru, P Ghenuche, D Stutman, A Boianu, M Risca, M Toma, C Petcu, G Acbas, S R Yoffe, A Noble, B Ersfeld, E Brunetti, R Capdessus, C Murphy, C P Ridgers, D Neely, S P D Mangles, R J Gray, A G R Thomas, J G Kirk, A Ilderton, M Marklund, D F Gordon, B Hafizi, D Kaganovich, J P Palastro, E D'Humieres, M Zepf, G Sarri, H Gies, F Karbstein, J Schreiber, G G Paulus, B Dromey, C Harvey, A Di Piazza, C H Keitel, M C Kaluza, S Gales, and N V Zamfir. High field physics and qed experiments at eli-np. *Romanian Reports in Physics*, 68:S145, 01 2016.

62. Zhijiang Chen, Sebastian Meuren, Elias Gerstmayr, Vitaly Yakimenko, Philip H. Bucksbaum, David A. Reis, and Representing The E-320 Collaboration. Preparation of Strong-field QED Experiments at FACET-II. In *Optica High-brightness Sources and Light-driven Interactions Congress 2022*, page HF4B.6, Budapest, 2022. Optica Publishing Group. ISBN 978-1-957171-06-7. doi: 10.1364/HILAS.2022.HF4B.6. URL https://opg.optica.org/abstract.cfm?URI=HILAS-2022-HF4B.6.

63. LUXE Collaboration, H. Abramowicz, M. Almanza Soto, M. Altarelli, R. Aßmann, A. Athanassiadis, G. Avoni, T. Behnke, M. Benettoni, Y. Benhammou, J. Bhatt, T. Blackburn, C. Blanch, S. Bonaldo, S. Boogert, O. Borysov, M. Borysova, V. Boudry, D. Breton, R. Brinkmann, M. Bruschi, F. Burkart, K. Büßer, N. Cavanagh, F. Dal Corso, W. Decking, M. Deniaud, O. Diner, U. Dosselli, M. Elad, L. Epshteyn, D. Esperante, T. Ferber, M. Firlej, T. Fiutowski, K. Fleck, N. Fuster-Martinez, K. Gadow, F. Gaede, A. Gallas, H. Garcia Cabrera, E. Gerstmayr, V. Ghenescu, M. Giorato, N. Golubeva, C. Grojean, P. Grutta, G. Grzelak, J. Hallford, L. Hartman, B. Heinemann, T. Heinzl, L. Helary, L. Hendriks, M. Hoffmann, D. Horn, S. Huang, X. Huang, M. Idzik, A. Irles, R. Jacobs, B. King, M. Klute, A. Kropf, E. Kroupp, H. Lahno, F. Lasagni Manghi, J. Lawhorn, A. Levanon, A. Levi, L. Levinson, A. Levy, I. Levy, A. Liberman, B. Liss, B. List, J. List, W. Lohmann, J. Maalmi, T. Madlener, V. Malka, T. Marsault, S. Mattiazzo, F. Meloni, D. Miron, M. Morandin, J. Moroń, J. Nanni, A. T. Neagu, E. Negodin, A. Paccagnella, D. Pantano, D. Pietruch, I. Pomerantz, R. Pöschl, P. M. Potlog, R. Prasad, R. Quishpe, E. Ranken, A. Ringwald, A. Roich, F. Salgado, A. Santra, G. Sarri, A. Sävert, A. Sbrizzi, S. Schmitt, I. Schulthess, S. Schuwalow, D. Seipt, G. Simi, Y. Soreq, D. Spataro, M. Streeter, K. Swientek, N. Tal Hod, T. Teter, A. Thiebault, D. Thoden, N. Trevisani, R. Urmanov, S. Vasiukov, S. Walker, M. Warren, M. Wing, Y. C. Yap, N. Zadok, M. Zanetti, A. F. Żarnecki, P. Zbińkowski, K. Zembaczyński, M. Zepf, D. Zerwas, W. Ziegler, and M. Zuffa. Technical Design Report for the LUXE experiment. *The European Physical Journal Special Topics*, 233(10):1709–1974, October 2024. ISSN 1951-6355, 1951-6401. doi: 10.1140/epjs/s11734-024-01164-9. URL https://link.springer.com/10.1140/epjs/s11734-024-01164-9.

64. E. E. Los, E. Gerstmayr, C. Arran, M. J. V. Streeter, C. Colgan, C. C. Cobo, B. Kettle, T. G. Blackburn, N. Bourgeois, L. Calvin, J. Carderelli, N. Cavanagh, S. J. D. Dann A. Di Piazza, R. Fitzgarrald, A. Ilderton, C. H. Keitel, M. Marklund, P. McKenna, C. D. Murphy, Z. Najmudin, P. Parsons, P. P. Rajeev, D. R. Symes,

M. Tamburini, A. G. R. Thomas, J. C. Wood, M. Zepf, G. Sarri, C. P. Ridgers, and S. P. D Mangles. Observation of quantum effects on radiation reaction in strong fields, 2024. URL https://arxiv.org/abs/2407.12071.

65. Aimé Matheron, Jean-Raphaël Marquès, Vincent Lelasseux, Yinren Shou, Igor A. Andriyash, Vanessa Ling Jen Phung, Yohann Ayoul, Audrey Beluze, Ioan Dăncuş, Fabien Dorchies, Flanish D'Souza, Mathieu Dumergue, Mickaël Frotin, Julien Gautier, Fabrice Gobert, Marius Gugiu, Santhosh Krishnamurthy, Ivan Kargapolov, Eyal Kroupp, Livia Lancia, Alexandru Lazăr, Adrien Leblanc, Mohamed Lo, Damien Mataja, François Mathieu, Dimitrios Papadopoulos, Pablo San Miguel Claveria, Kim Ta Phuoc, Anda-Maria Talposi, Sheroy Tata, Călin A. Ur, Daniel Ursescu, Lidia Văsescu, Domenico Doria, Victor Malka, Petru Ghenuche, and Sebastien Corde. Compton photons at the gev scale from self-aligned collisions with a plasma mirror, 2024. URL https://arxiv.org/abs/2412.19337.

66. T. Heinzl, B. King, and A. J. MacLeod. Locally monochromatic approximation to QED in intense laser fields. *Physical Review A*, 102(6):063110, December 2020. ISSN 2469-9926, 2469-9934. doi: 10.1103/PhysRevA.102.063110. URL https://link.aps.org/doi/10.1103/PhysRevA.102.063110.

67. A. Di Piazza, M. Tamburini, S. Meuren, and C. H. Keitel. Improved local-constant-field approximation for strong-field QED codes. *Physical Review A*, 99(2):022125, February 2019. ISSN 2469-9926, 2469-9934. doi: 10.1103/PhysRevA.99.022125. URL https://link.aps.org/doi/10.1103/PhysRevA.99.022125.

68. M. Kh. Khokonov and H. Nitta. Standard Radiation Spectrum of Relativistic Electrons: Beyond the Synchrotron Approximation. *Physical Review Letters*, 89(9):094801, August 2002. ISSN 0031-9007, 1079-7114. doi: 10.1103/PhysRevLett.89.094801. URL https://link.aps.org/doi/10.1103/PhysRevLett.89.094801.

69. A. Ilderton, B. King, and D. Seipt. Extended locally constant field approximation for nonlinear Compton scattering. *Physical Review A*, 99(4):042121, April 2019. ISSN 2469-9926, 2469-9934. doi: 10.1103/PhysRevA.99.042121. URL https://link.aps.org/doi/10.1103/PhysRevA.99.042121.

70. T. Podszus and A. Di Piazza. High-energy behavior of strong-field QED in an intense plane wave. *Physical Review D*, 99(7):076004, April 2019. ISSN 2470-0010, 2470-0029. doi: 10.1103/PhysRevD.99.076004. URL https://link.aps.org/doi/10.1103/PhysRevD.99.076004.

71. E.G. Gelfer, A.M. Fedotov, A.A. Mironov, and S. Weber. Nonlinear Compton scattering in time-dependent electric fields beyond the locally constant crossed field approximation. *Physical Review D*, 106(5):056013, September 2022. ISSN 2470-0010, 2470-0029. doi: 10.1103/PhysRevD.106.056013. URL https://link.aps.org/doi/10.1103/PhysRevD.106.056013.

72. Wenqi Li, Zebiao Gan, Lianghong Yu, Cheng Wang, Yanqi Liu, Zhen Guo, Lu Xu, Min Xu, Yin Hang, Yi Xu, Jianye Wang, Pei Huang, He Cao, Bo Yao, Xiaobo Zhang, Lingru Chen, Yunhai Tang, Shuai Li, Xingyan Liu, Shanming Li, Mingzhu He, Dinjun Yin, Xiaoyan Liang, Yuxin Leng, Ruxin Li, and Zhizhan Xu. 339 J high-energy Ti:sapphire chirped-pulse amplifier for 10 PW laser facility. *Optics Letters*, 43(22):5681, November 2018. ISSN 0146-9592, 1539-4794. doi: 10.1364/OL.43.005681. URL https://opg.optica.org/abstract.cfm?URI=ol-43-22-5681.

73. Edwin Cartlidge. The light fantastic. *Science*, 359 (6374):382–385, 2018. doi: 10.1126/science.359.6374.382. URL https://www.science.org/doi/abs/10.1126/science.359.6374.382.

74. K. Burdonov, A. Fazzini, V. Lelasseux, J. Albrecht, P. Antici, Y. Ayoul, A. Beluze, D. Cavanna, T. Ceccotti, M. Chabanis, A. Chaleil, S. N. Chen, Z. Chen, F. Consoli, M. Cuciuc, X. Davoine, J. P. Delaneau, E. d'Humières, J.-L. Dubois, C. Evrard, E. Filippov, A. Freneaux, P. Forestier-Colleoni, L. Gremillet, V. Horny, L. Lancia, L. Lecherbourg, N. Lebas, A. Leblanc, W. Ma, L. Martin, F. Negoita, J.-L. Paillard, D. Papadopoulos, F. Perez, S. Pikuz, G. Qi, F. Quéré, L. Ranc, P.-A. Söderström, M. Scisciò, S. Sun, S. Vallières, P. Wang, W. Yao, F. Mathieu, P. Audebert, and J. Fuchs. Characterization and performance of the Apollon short-focal-area facility following its commissioning at 1 PW level. *Matter and Radiation at Extremes*, 6(6):064402, November 2021. ISSN 2468-2047, 2468-080X. doi: 10.1063/5.0065138. URL https://pubs.aip.org/mre/article/6/6/064402/253220/Characterization-and-performance-of-the-Apollon.

75. M. Aléonard, M. Altarelli, Patrizio Antici, Alexander Apolonskiy, Patrick Audebert, Andrzej Bartnik, C. Barty, A. Bernstein, Jens Biegert, P. Böni, Nicola Booth, D. Bote, Sergei Bulanov, Rytis Butkus, Luis Cardoso, J.P. Chambaret, D. Charambilidis, G. Cheriaux, R. Clarke, and Matt Zepf. *WHITEBOOK ELI – Extreme Light Infrastructure; Science and Technology with Ultra-Intense Lasers*. 01 2011. doi: 10.13140/2.1.1227.0889.

76. Christophe Radier, Olivier Chalus, Mathilde Charbonneau, Shanjuhan Thambirajah, Guillaume Deschamps, Stephane David, Julien Barbe, Eric Etter, Guillaume Matras, Sandrine Ricaud, Vincent Leroux, Caroline Richard, François Lureau, Andrei Baleanu, Romeo Banici, Andrei Gradinariu, Constantin Caldararu, Cristian Capiteanu, Andrei Naziru, Bogdan Diaconescu, Vicentiu Iancu, Razvan Dabu, Daniel Ursescu, Ioan Dancus, Calin Alexandru Ur, Kazuo A. Tanaka, and Nicolae Victor Zamfir. 10 PW peak power femtosecond laser pulses at ELI-NP. *High Power*

https://doi.org/10.1017/hpl.2025.36 Published online by Cambridge University Press

Laser Science and Engineering, 10:e21, 2022. ISSN 2095-4719, 2052-3289. doi: 10.1017/hpl.2022.11. URL https://www.cambridge.org/core/product/identifier/S2095471922000111/type/journal_article.

77. J. D. Zuegel, S.-W. Bahk, I. A. Begishev, J. Bromage, C. Dorrer, A. V. Okishev, and J. B. Oliver. Status of High-Energy OPCPA at LLE and Future Prospects. In *CLEO: 2014*, page JTh4L.4, San Jose, California, 2014. OSA. ISBN 978-1-55752-999-2. doi: 10.1364/CLEO_AT.2014.JTh4L.4. URL https://opg.optica.org/abstract.cfm?URI=CLEO_AT-2014-JTh4L.4.
78. V. I. Ritus. Quantum effects of the interaction of elementary particles with an intense electromagnetic field. *Journal of Soviet Laser Research*, 6(5):497–617, 1985. ISSN 0270-2010, 1573-8760. doi: 10.1007/BF01120220. URL http://link.springer.com/10.1007/BF01120220.
79. A. Di Piazza, K. Z. Hatsagortsyan, and C. H. Keitel. Quantum Radiation Reaction Effects in Multiphoton Compton Scattering. *Physical Review Letters*, 105(22):220403, November 2010. ISSN 0031-9007, 1079-7114. doi: 10.1103/PhysRevLett.105.220403. URL https://link.aps.org/doi/10.1103/PhysRevLett.105.220403.
80. A. Di Piazza. Exact Solution of the Landau-Lifshitz Equation in a Plane Wave. *Letters in Mathematical Physics*, 83(3):305–313, March 2008. ISSN 0377-9017, 1573-0530. doi: 10.1007/s11005-008-0228-9. URL http://link.springer.com/10.1007/s11005-008-0228-9.
81. I. V. Khutoretsky. Design of an optimal ross filter system for x-ray spectra measurements in the range of 8.98–88 kev. *Review of Scientific Instruments*, 66(1):773–775, 01 1995. ISSN 0034-6748. doi: 10.1063/1.1146285. URL https://doi.org/10.1063/1.1146285.
82. T. Bonnet, M. Comet, D. Denis-Petit, F. Gobet, F. Hannachi, M. Tarisien, M. Versteegen, and M. M. Aléonard. Response functions of imaging plates to photons, electrons and 4he particles. *Review of Scientific Instruments*, 84(10):103510, 10 2013. ISSN 0034-6748. doi: 10.1063/1.4826084. URL https://doi.org/10.1063/1.4826084.

https://doi.org/10.1017/hpl.2025.36 Published online by Cambridge University Press